Journal of Applied Fluid Mechanics, Vol. 17, No. 2, pp. 337-351, 2024.
Available online at www.jafmonline.net, ISSN 1735-3572, EISSN 1735-3645.
https://doi.org/10.47176/jafm.17.02.2127

Investigation on Aerodynamic Robustness of Compressor Blade with Asymmetric Leading Edge

G. Yang, L. Gao†, C. Ma, H. Wang and N. Ge

School of Power and Energy, Northwestern Polytechnical University, Xi'an, Shaanxi, 710129, China
The National Key Laboratory of Aerodynamic Design and Research, Xi'an, Shaanxi, Zip 710129, China

†Corresponding Author Email: gaolm@nwpu.edu.cn

ABSTRACT

To improve the aerodynamic characteristics of compressor blades, a novel asymmetric leading edge (ASYLE) has been introduced and shown to offer superior performance. However, the aerodynamic robustness of such specially designed leading edge (LE) remains unclear due to the considerable uncertainty problems it presents. This paper investigates the robustness of ASYLE blade under both geometric and operational uncertainties. Profile deviations within ±0.05mm were introduced to investigate the influence of manufacturing errors. In addition, the perturbated inflow angles between ±0.375° were considered for uncertain inflow conditions. The statistic aerodynamic performance as well as operating dispersibilities at Ma=0.7 were obtained by the non-intrusive polynomial chaos (NIPC) method. The results show that considering uncertain profile errors, the operating range of ASYLE blade is 2.3° wider than original leading edge (ORILE) blade and the dispersion of total pressure loss can be reduced by 53.1% at β_1=45.8°. Regarding uncertain inflow angle variations, the total pressure loss dispersion of ASYLE blade can be reduced by 93.8% at β_1=50.8°. The ASYLE shows better overall aerodynamic robustness than ORILE upon considering uncertainty limits. The influence propagations in the flow fields of both uncertainties were further analysed, which revealed that the variations of separation bubble structure near LE are the direct cause to the aerodynamic uncertainties. The ASYLE design effectively controls the size and variation of LE separation bubble and thus demonstrates better aerodynamic robustness.

Article History

Received June 28, 2023
Revised August 27, 2023
Accepted October 5, 2023
Available online December 4, 2023

Keywords:

Asymmetric leading edge
Aerodynamic robustness
Profile error
Inflow angle perturbation
Uncertainty quantification

1. INTRODUCTION

The leading edge (LE) of a compressor blade is a crucial component that directly impacts its downstream boundary layer and plays a significant role in compressor flow. The LE flow is complex and delicate. Separate flows often occur at the LE. Cumpsty (2004) proposed that LE separation would result in an earlier boundary transition from laminar to turbulent. Walravens's measurements (Walraevens & Cumpsty, 1995) showed that LE separation bubbles led to a thicker boundary layer and higher loss, which was as much as 32% according to Wheeler et al. (2009). In addition to the flow separation, a sharp pressure change, known as the suction spike (Carter, 1961), also appears at LE. The suction spike has been identified as having a significant effect on inducing separation and transition (Wheeler & Miller, 2008), and it has been considered a new performance criterion for compressor blades (Goodhand & Miller, 2009). Accordingly, the flow of compressor blade LE is essential, and the design of the LE profile is a key step in the blade design procedure.

By improving the design of the LE profile shape, the LE flow can be effectively optimized. The typical LE profile shapes are essentially circular, which is convenient for design and manufacturing. According to Liu's experiments (Liu et al. 2003), compared to a circular LE, an elliptical LE can more effectively suppress the separation bubble and is more adaptable to incidence changes. Goodhand (2010) proved that the elliptical LE design can reduce the LE suction spike intensity and achieve laminar flow on the blade surface. This work also indicated that the curvature discontinuity at the junction between the LE and blade body should be avoided and developed a continuous curvature LE design, which has a lower suction spike than elliptical LE. Continuous

NOMENCLATURE

LE	Leading Edge	NIPC	Non-intrusive Polynomial Chaos
ASYLE	asymmetric leading edge	UQ	Uncertainty Quantification
ORILE	original leading edge	DNS	Direct Numerical Simulation
SST	Shear Stress Transport	LES	Large Eddy Simulation
SSLCC	Shear-Sensitive Liquid Crystal Coating	RANS	Reynolds-Average Navier-Stokes
NUM	numerical	PSLE	Pressure Side Leading Edge
EXP	experimental	SSLE	Suction Side Leading Edge
Ma_1	inflow Mach number	e	profile error
i	incidence angle	f	inflow angle perturbation
C	chord length	μ	mean value
τ	solidity	σ	standard deviation
$\beta_{1\text{des}}$	design inflow angle	d	performance dispersibility
β_1	inflow angle	C_P	static pressure coefficient
ϖ	total pressure loss	x/a	normalized arc length
L	separation bubble length	H	separation bubble maximum thickness

curvature LE design methods began to be developed. Zhang et al. (2012) used a polynomial-based LE design method to achieve curvature continuity, resulting in a 10% decrease in total loss. Song et al. (2014) proposed a continuous curvature LE design method that increased the blade's operating incidence range by 1.2° compared to the elliptical LE. The benefits of the continuous curvature LE design have also been demonstrated in other works (Hamakhan & Korakianitis, 2010; Liu et al., 2013; Cui et al., 2019).

Subsequently, considering the flow feature differences between the suction surface and pressure surface of the compressor blade, the asymmetric leading edge (ASYLE) design was introduced (Lu & Xu, 2003). In this new design, the profile shapes of the suction side leading edge (SSLE) and pressure side leading edge (PSLE) were separately designed (Yang et al., 2020, 2021), and the LE curvature distribution was intentionally arranged (Yang et al., 2022) for better control of the LE flow. The ASYLE design showed better abilities to eliminate the separation bubble and weaken the suction spike than the symmetric curvature continuous LE at high incidence and thus had better aerodynamic performance and a wider operational range (Hanson et al., 2012; Yang et al., 2022).

To date, the strengths of the novel design have only been proven by computational fluid dynamics (CFD) or laboratory experiments under ideal conditions. However, in practical applications, compressor blades are faced with many uncertainty problems. The LE of compressor blades is one of the most difficult parts to manufacture, and inevitable manufacturing errors lead to unexpected profile deviations from the intended design, which brings uncertainties to the geometric profile of the actual LE (Garzón, 2002; Lejon et al., 2020). Goodhand et al. (2015) indicated that the manufacturing variations around LE lead to a 10% reduction in the blade's positive incidence range. Ma et al. (2021) examined the influence of LE with real manufacturing errors and found that the uncertain LE radius and wedge angle are the most sensitive factors affecting aerodynamic performance. Gao et al. (2023) stated that blades may fail to meet the aerodynamic qualification with LE manufacturing uncertainties.

In addition, the inflow perturbations of the compressor are considerable even during the cruising state due to turbulence (Nicholls et al., 1983) or the atmospheric environment (Ali & Kim 2020). The initial design process of LE is carried out under deterministic conditions, while realistic uncertain inflow will directly change the operating conditions of the compressor blade. The inflow uncertainties always lead to aerodynamic performance variations and dispersion from the intended design. Gao et al. (2022) showed that the fluctuation of the total pressure loss coefficient increased approximately 15.8 times under uncertain inflow Mach number and incidence conditions. Wang et al. (2023) pointed out that uncertainties of incidence caused large perturbations in LE flow, which led to overall performance degradation and performance dispersion, and the probabilities that the actual total pressure loss coefficient was higher than the nominal value were 83.6% and 69.9%, respectively. Guo et al. (2023) revealed that under the perturbations of inlet incidences, the mean aerodynamic loss is always aggravated, and the variation in LE flow is the main factor driving the variation in aerodynamic performance when the inlet incidence is perturbed.

These studies emphasize that LE flows are highly sensitive to geometrical uncertainties caused by machining errors and operational uncertainties caused by inflow perturbations, which collectively lead to a sharp deterioration of compressor blade aerodynamic performance. Consequently, for a novel LE design, it is necessary to evaluate the aerodynamic robustness against those uncertainties before implanting such a design in practical service. To the best of our knowledge, there are few reports that currently describe such research. In this paper, a novel ASYLE profile (as designed previously) is studied for its aerodynamic robustness under machining errors and inflow perturbations to determine whether or not such refined LE design will lead to a decline in robustness. This paper contains the following contributions. First, a set of uncertainty quantification (UQ) procedures based on non-intrusive polynomial chaos (NIPC) and CFD is proposed, and two research models of profile uncertainty and inflow angle uncertainty are established for the ASYLE blade. Second, the performance dispersibilities and statistical performances under two kinds of uncertainties are obtained to evaluate

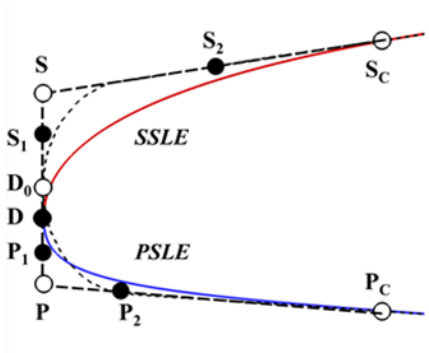

Fig. 1 ASYLE design schematic diagram

the aerodynamic robustness of the ASYLE blade in comparison with the original LE. Third, the propagations of two kinds of uncertainties in the LE flow field and their mechanisms on aerodynamic robustness are analysed. The key factors of LE flow robustness are discussed, which may provide inspiration for robust LE design.

2. INTRODUCTION OF ASYLE DESIGN AND ITS GEOMETRIC FEATURES

The ASYLE design was made for a high subsonic compressor blade. Its chord length (C) is 69.94mm, solidity (τ) is 2.3 and design inflow angle β_{1des} is 48.3°. The original leading edge (ORILE) shape of the blade is circular, and its radius is 0.52mm. The ASYLE design was carried out on the compressor blade, and a schematic diagram of the design method is shown in Fig.1.

A brief review of the ASYLE design process is as follows. The LE curve is parameterized by two 3rd-order NURBS curves on each side. The ORILE profile is shown as a dotted line, and D_0 is the LE point. The design of the ASYLE is achieved by moving LE point D_0 along tangent line SP to offset point D. The SSLE curve is defined by control points D, S_1, S_2, and S_C. Moreover, the PSLE curve is defined by control points D, P_1, P_2 and P_C. Through the control point arrangement, diverse ASYLE profiles are generated. The results for which the curvatures at junctions D, S_C and P_C are consistent are selected to ensure that the ASYLE profiles obtained are curvature continuous.

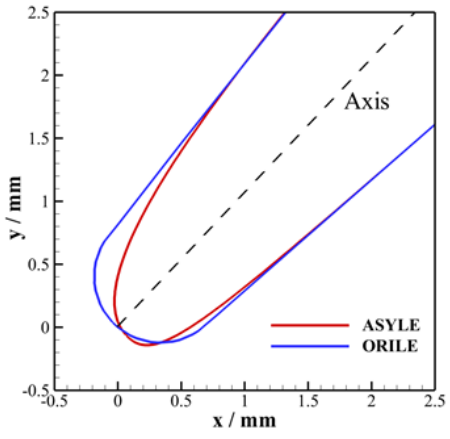

Fig. 2 Comparison of ASYLE and ORILE

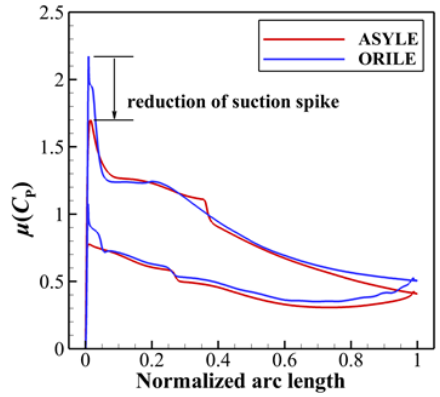

(a) Static pressure coefficient C_P comparison at β_1=50.8°

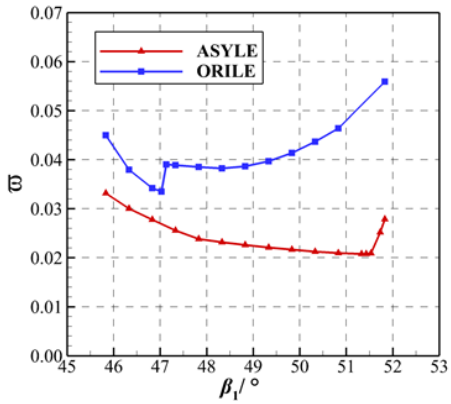

(b) Total pressure loss ϖ characteristics comparison

Fig. 3 Aerodynamic performance comparison of the ASYLE and CIRLE compressor blades

Figure 2 provides a profile comparison between the ORILE and the ASYLE design results. This comparison clearly illustrated that the SSLE and PSLE curves of ASYLE are distinct. The ASYLE design achieves a better arrangement of SSLE curvature with limited compromise of PSLE; thus, the curvature of the SSLE becomes more moderate, which helps to further restrain the LE suction spike and separation bubble. As shown in Fig. 3(a), the intensity of the suction spike can be reduced by 21.8% at β_1=50.8°. Therefore, the ASYLE greatly improves the aerodynamic performance of the compressor blade. Figure 3(b) shows that the total pressure loss ϖ is reduced by 54.8% at β_1=50.8°.

However, these conclusions were drawn from deterministic research. Figure 2 shows that the ASYLE has a larger LE point curvature, and its curvature radius is 0.34mm, while the curvature radius of ORILE is 0.52mm. Thus, the ASYLE profile shape is sharper than that of ORILE. Conventional wisdom would indicate that a sharper LE is more sensitive to inflow perturbations than blunt ones (Goodhand et al., 2012), so the aerodynamic robustness of the ASYLE might be reduced. Moreover, the profile shape of the ASYLE is more distinctive and special and seems less adaptive to uncertain geometry profile changes caused by manufacturing errors. Consequently, it is unclear whether or not the specific ASYLE is more robust, so an investigation of the aerodynamic robustness

of the ASYLE with a comparison of the ORILE is necessary.

3. RESEARCH METHODS FOR AERODYNAMIC ROBUSTNESS OF ASYLE COMPRESSOR BLADE

3.1 Uncertainty Quantification Method Based on NIPC

NIPC offers the advantage of high precision and timesaving compared with other UQ methods. The self-developed one-dimensional NIPC method (Ma et al., 2021) is used here to analyse the aerodynamic robustness of the ASYLE blade. This approach implements polynomials to expand the random variables, and the output expression of the system is established by solving the corresponding polynomial coefficients. The system output Y, such as velocity, pressure, or flow loss in a stochastic fluid dynamic problem, is expressed as

$$Y(x)=\sum_{i=0}^{Q-1} c_i \Psi_i(x) \tag{1}$$

where x is the random inputs following a probability distribution, such as the uncertain profile errors or the uncertain inflow angle deviations. c_i is the coefficient of each polynomial, and $\psi_i(x)$ is the polynomial function. For random variables that fit a Gaussian distribution, the Hermite orthogonal basis function is selected as the polynomial function. Q is the number of polynomials. According to previous works (Ma et al., 2021; Gao et al., 2022), the fourth-order (r = 4) NIPC was proven qualified to efficiently quantify the influence of uncertainties on compressor blade aerodynamic performance. The uncertain problem solved in this paper concerns a single variable each time, and the term Q = 5 is obtained through Eq. (2)

$$Q=\frac{(1+r)!}{r!} \tag{2}$$

Deterministic coefficients c_i can be solved by using the Galerkin projection:

$$c_i=\frac{1}{\langle \Psi_i, \Psi_i \rangle}\int_{\Omega} Y(x)\Psi_i(x)w(x)dx \tag{3}$$

where $<\cdot,\cdot>$ represents the inner product, and $w(x)$ is the weight over the support domain Ω.

By solving for these polynomial coefficients, the relationship of system output Y and random input variable x is constructed. Then, the mean value $\mu(Y)$ and the standard deviation $\sigma(Y)$ of stochastic output Y is calculated by

$$\mu(Y)=c_0 \tag{4}$$

$$\sigma^2(Y)=\sum_{i=1}^{Q-1}\left[c_i^2\langle \Psi_i^2(x)\rangle\right] \tag{5}$$

For the uncertain problems studied here, the random input variable x is the profile error e and the inflow angle perturbation f. The system output Y can be the total pressure loss coefficient, static pressure ratio or other flow field aerodynamic parameters.

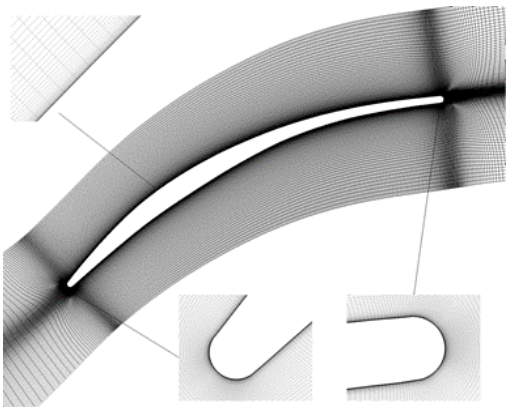

Fig. 4 Computation mesh for compressor blade

3.2 CFD Method for Deterministic Performance Prediction and Validation

In the UQ of a compressor blade, CFD is used as the transfer function to establish the corresponding relationship between random input variables and the aerodynamic performance system response. As the magnitude of the profile error defined is relatively small, the adopted CFD method should be capable of capturing tiny differences accurately. Simultaneously, because LE flow has a great influence on downstream boundary layer growth and development, the adopted numerical method should be capable of predicting LE separation and boundary layer transition. Although direct numerical simulation (DNS) or large eddy simulation (LES) offer higher precision, they are too time-consuming to acquire sufficient performance characteristics in UQ studies. Considering the accuracy and efficiency, the k-ω based shear stress transport (SST) Reynolds-average Navier–Stokes (RANS) model coupled with the γ-Re_θ transition model (Menter et al., 2004; Langtry et al., 2004) was adopted. This method has been widely used in LE separation and transition predictions and has proven effective (Zhang et al., 2012; Song et al., 2014; Cui et al., 2019).

The O4H type computation mesh was generated and is shown in Fig.4. The grid scale of the first layer near the wall was set to 1×10^{-6}m, which guarantees $y^+\leq1$. The grid growth factor was 1.1 to ensure that the boundary layer region had more than 30 layers grid. The total number of computational domain nodes was 192,538. Numerical calculations were conducted by the CFX module of ANSYS software. The inflow angle β_1, total temperature and total pressure were given as the inlet conditions, and the mass flow rate was set as outlet conditions. Periodic boundaries were given in the pitchwise direction, and the symmetry boundaries were set at endwalls to ensure 2D calculations. Through the adjustment of the mass flow rate at the outlet, the target Mach number of incoming flows Ma_1 were thus attained.

To validate the method, numerical calculations were carried out on the research blade at Ma_1=0.5 and β_1 = 48.3°. The distribution of the total pressure loss ϖ at the downstream exit was compared with the experimental measurement results (Ma et al., 2017). Both the experimental and numerical total pressure loss ϖ are calculated

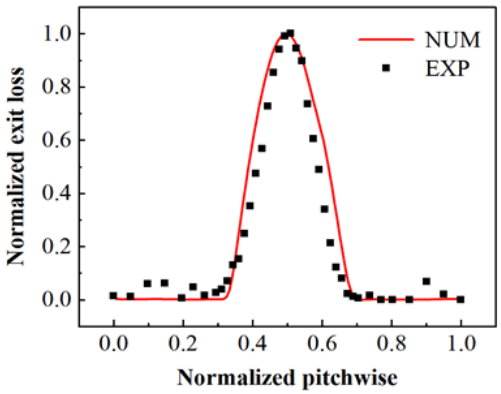

Fig. 5 Comparison of exit loss prediction between the numerical and experimental methods

Table 1 Comparison of flow regime change prediction between numerical and experimental methods

Position	NUM	EXP	Deviation
LE separation reattachment	5.7%*C*	5.2%*C*	0.5%*C*
Transition start	58.3%*C*	5.7%*C*	0.6%*C*
Transition end	69.7%*C*	69.4%*C*	0.3%*C*

by Eq. (6).

$$\varpi = \frac{p_1^* - p_2^*}{p_1^* - p_1} \tag{6}$$

p_1^*, p_1, and p_2^* represent the inlet total pressure, inlet static pressure and outlet total pressure, respectively. The outlet total pressure p_2^* is measured at one chordwise direction down to the trailing edge at the mid span of the blade.

As demonstrated in Fig.5, the normalized exit loss distribution along the pitch of the numerical calculation has great consistency with the experimental results. Furthermore, it is necessary to validate the prediction accuracy for boundary regime changes. The numerical calculation was performed on the blade in a shear-sensitive liquid crystal coating (SSLCC) experiment (Li et al., 2018). The positions of flow regime change obtained by experiment and numerical calculation are compared (Yang et al., 2022) and shown in Table 1. The deviations of the flow regime transformation prediction were no more than 0.6%. The numerical method there is shown to have sufficient capability to predict the boundary layer flow regime variation, including separation and transition.

4. ESTABLISHMENT OF MANUFACTURING AND INFLOW UNCERTAINTY MODELS

4.1 Profile Uncertainty Models with Random Manufacturing Errors

Blade profile errors are inevitable outcomes of the blade machining process. A tolerance range is always given and maintained in manufacturing, and the profile

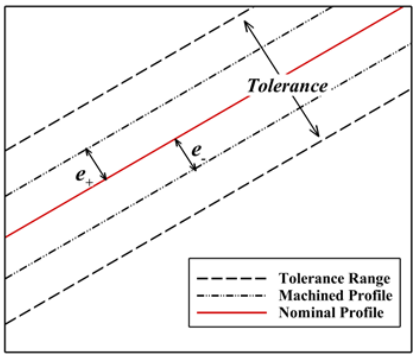

Fig. 6 Schematic diagram of the tolerance range and profile errors

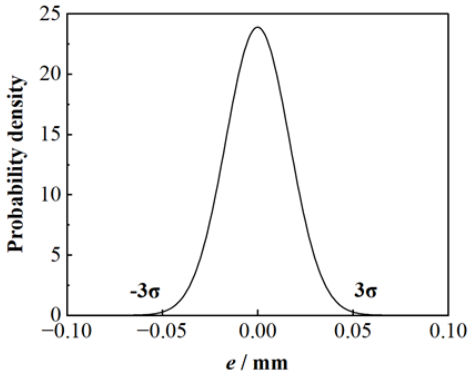

Fig. 7 PDF of profile errors distribution

errors of the machined blades are included within this tolerance, as shown in Fig.6. However, in the quantitative analysis of the influence of uncertain profile errors on aerodynamic robustness, only knowing the tolerance range is not enough, and the profile error value distribution within the tolerance range should also be specified. Because our purpose is to carry out theoretically comparative research, the distribution of profile error values can be expressed as a probability density function (PDF). A previous study found that the profile errors approximately satisfy the Gaussian distribution within the tolerance range (Ma et al., 2021). Consequently, the profile errors were presumed to follow a Gaussian distribution. The tolerance range was chosen to be ±0.05mm. Considering the characteristic of the Gaussian distribution that $\pm 3\sigma$ covers over 99.7% of the whole probability, 3σ was 0.05mm, so the profile errors e here satisfies the $N(0, 0.0167^2)$ Gaussian distribution, as shown in Fig.7.

The random error e was applied to the ideal ASYLE profile. To maintain the smoothness and continuity of the blade surface, the same profile error e was also added to the blade main body. The profile errors at the LE and the blade body are assumed to be equal to reduce irrelevant issues and improve the efficiency of aerodynamic UQ analysis. This assumption has been widely used in engineering, including many relevant studies (Gao et al., 2019; Liu et al., 2021; Guo et al., 2022). One of these works concluded that the uniform profile error could be used to estimate the influence of manufacturing uncertainty on aerodynamic robustness (Liu et al., 2021), which illustrates the rationality of the assumption.

4.2 Inflow Uncertainty Models with Random Inflow Angle Perturbations

Inflow angle perturbation inevitably occurs during flight and is one of the most significant inflow uncertainties. To quantitatively analyse the influence of uncertain inflow angle perturbations, a theoretical PDF distribution model was also adopted for ASYLE blades. A real-time measurement of inflow angle β_1 was carried out in a continuous high subsonic cascade wind tunnel, and the probability distribution of the inflow angle was distinguished by the Kolmogorov–Smirnov (K-S) test (Gao et al., 2022). The results show that the inflow angles perturbed randomly around the nominal value within a certain range, as demonstrated in Fig.8, and the results also show that the PDF of inflow angle perturbations agrees with a Gaussian distribution $N(\mu, \sigma^2)$ around the nominal value. Considering the statistical results in the experiment, σ=0.125° was set. Consequently, the uncertain inflow angle perturbation f here satisfies the $N(0, 0.125^2)$ Gaussian distribution and varies randomly within ±0.375° around the nominal inflow angle, as shown in Fig.9. The random perturbation f was added to the ideal nominal inflow angle to attain the real inflow angle β_1.

As mentioned in Section 3.1, fourth-order (r = 4) NIPC was chosen to quantify the aerodynamic characteristics of the ASYLE blade under uncertain profile errors and inflow angle perturbations. Based on the polynomial coefficient solving requirements, for each blade, five deterministic results at the integral nodes were numerically investigated under the inlet Mach number Ma_1=0.7, these results consisting of two positive error samples, two negative error samples and one nominal sample. The polynomial coefficients were solved as Section 3.1 illustrates. Then, the relationship of system output Y and random input variable x is built, and the mean value $\mu(Y)$ and the standard deviation $\sigma(Y)$ of a stochastic output Y is acquired.

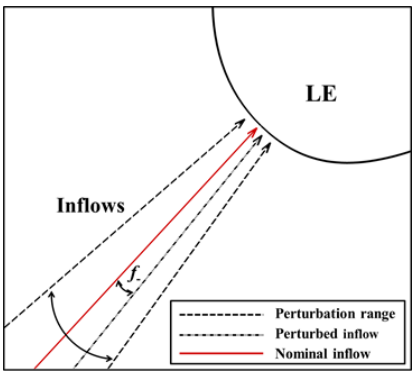

Fig. 8 Schematic diagram of inflow angle perturbations

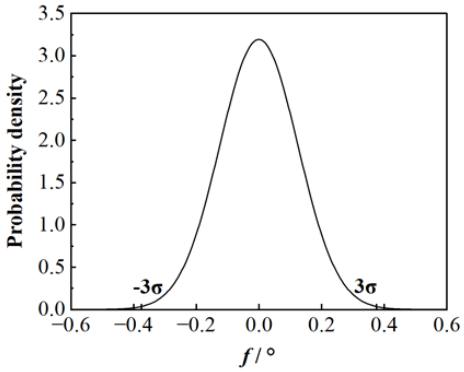

Fig. 9 PDF of inflow angle perturbations distribution

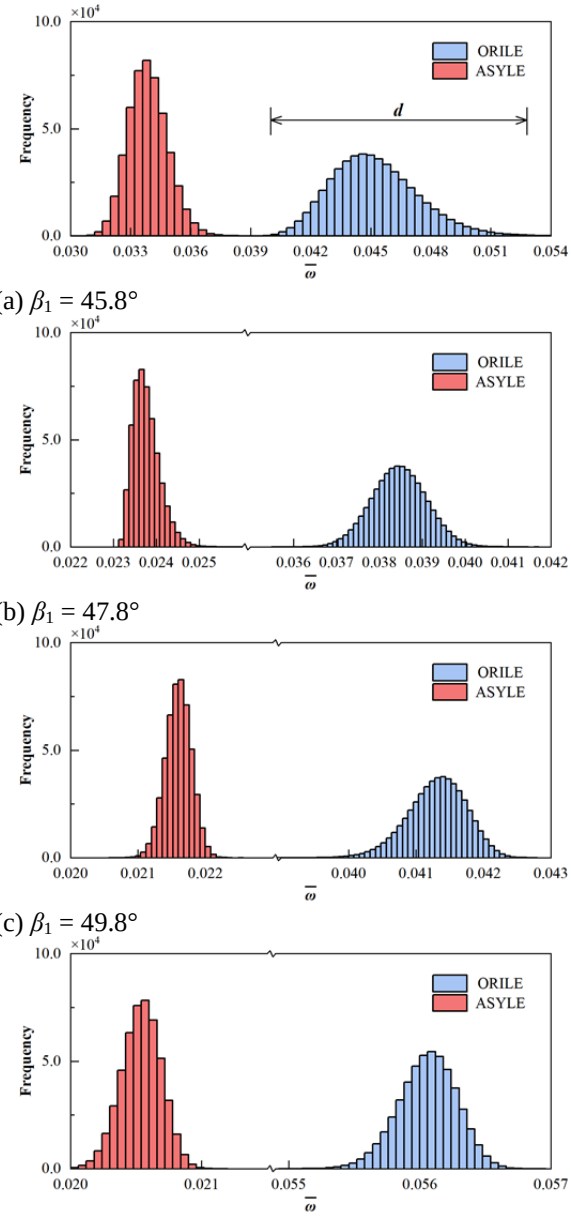

Fig. 10 Frequency distribution comparison of performance under profile errors

5. INFLUENCE OF UNCERTAIN PROFILE ERRORS ON AERODYNAMIC ROBUSTNESS

5.1 Influence of Uncertain Profile Errors on Performance Characteristics

To investigate the specific performance output of the ASYLE blade under uncertain profile errors, the frequency distribution histogram graphs of the total pressure loss ϖ of the ASYLE blade are given in Fig.10 and are compared with the ORILE blade. These results

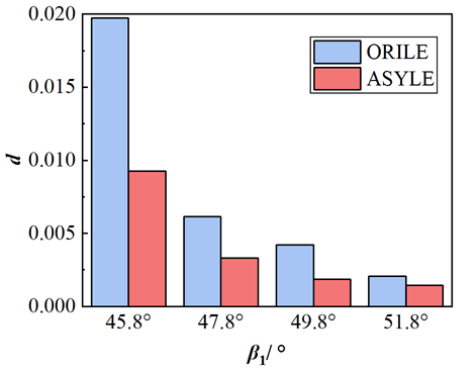

Fig. 11 Performance dispersibility comparison under uncertain profile errors

were derived through the NIPC model built at each inlet flow condition, and the input profile error e of each NIPC model was generated with the Latin hypercube sampling (LHS) method based on the assumed Gaussian distributed profile errors described in Section 4.1. The number of samples is 5.0×10^5. Figure 10 clearly shows the total pressure loss distributions for both blades under different inflow angles. The sharper the distribution figure is, the more concentrated the performance is. This result shows that the performance of the ASYLE blade is more stable under different working conditions, but the corresponding difference decreases with β_1. We observe that the output form is not normally distributed, with some concentration and bias, although the input profile error e is Gaussian distributed.

To quantitatively describe the performance dispersion under uncertain profile errors, the range of the total pressure loss distribution is defined as the dispersibility $d(\varpi)$, as shown in Fig.10. The performance dispersibility comparison in Fig.11 illustrates that for both blades, the performance dispersibilities caused by uncertain profile errors are more evident at a small inflow angle $\beta_1 = 45.8°$, and the total pressure loss dispersion of the ASYLE blade decreases by 53.1% relative to the ORILE blade. As β_1 increases, the effect of the profile error decreases, and the improvement of the ASYLE blade also decreases.

The statistical performance features of the ASYLE blade with uncertain profile errors are further analysed. The characteristics of the total pressure loss mean value $\mu(\varpi)$ of the ASYLE blade are given in Fig.12(a), superimposed with the standard deviation σ marked in grey, and are compared with the ORILE blade. As shown, with the inclusion of profile errors, the $\mu(\varpi)$ of the ASYLE blade remains much smaller than that of the ORILE blade on the whole. Moreover, the existence of profile error always leads to a decrease in the blade working range. Figure 12(a) reveals that under the same level of uncertain profile errors, the operating range of the ASYLE blade is wider and extends 0.5° at small inflow angles and 1.8° at large inflow angles. Even so, the ASYLE blade still presents clear advantages in overall aerodynamic performance upon considering the uncertain profile errors.

The standard deviation of the total pressure loss $\sigma(\varpi)$ comparison is given in Fig. 12(b). The $\sigma(\varpi)$ of ASYLE is below that of ORILE, which means that the performance

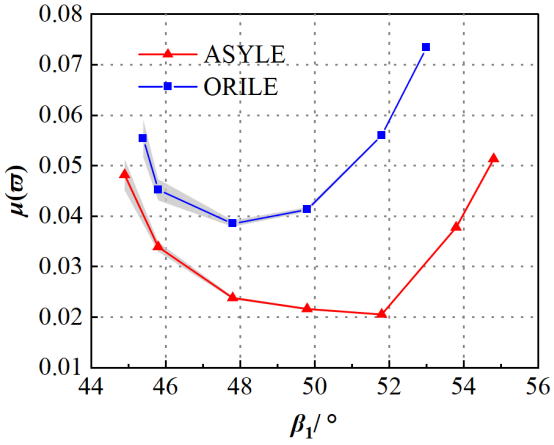

(a) Mean value of total pressure loss $\mu(\varpi)$ comparison

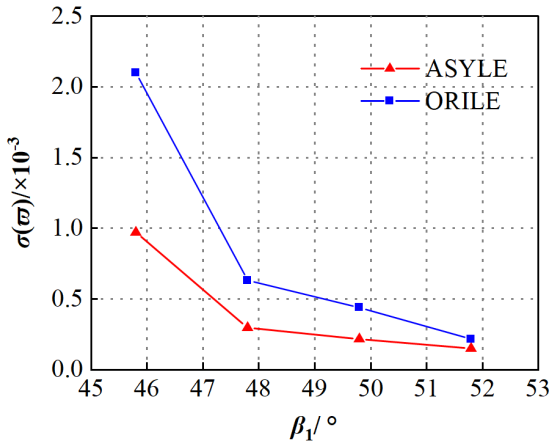

(b) Standard deviation of total pressure loss $\sigma(\varpi)$ comparison

Fig. 12 Comparison of total pressure loss characteristics under uncertain profile errors

deviation caused by uncertain profile errors of ASYLE is less than that of ORILE, so the ASYLE blade has more robustness. Moreover, $\sigma(\varpi)$ decreases with the inflow angle β_1 for both blades, and the difference between the two blades also decreases. This result illustrates that for the studied blade in this work, the influence of profile error is more prominent at small inflow angles or negative incidences. The ASYLE blade significantly diminishes the influence of profile errors, and the $\sigma(\varpi)$ of the ASYLE blade is reduced by 53.8% at $\beta_1 = 45.8°$ compared with the ORILE blade.

5.2 Influence of Uncertain Profile Errors on the Flow Field and Mechanism Analysis

According to previous results, the influence of profile error is much more distinct at smaller inflow angles, which are also improved most with the design of the ASYLE. To examine the propagation difference of uncertain profile errors in the flow field, the distribution of the total pressure loss standard deviation $\sigma(\varpi)$ for both blades at β_1=45.8° is presented in Fig.13. The local high value reveals the large variation amplitude area of the total pressure loss ϖ with uncertain profile errors.

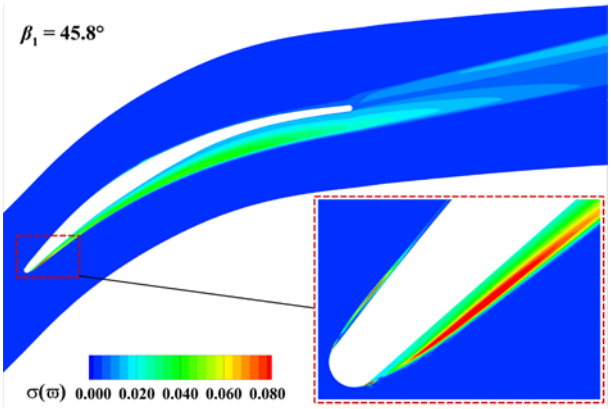

(a) ORILE blade

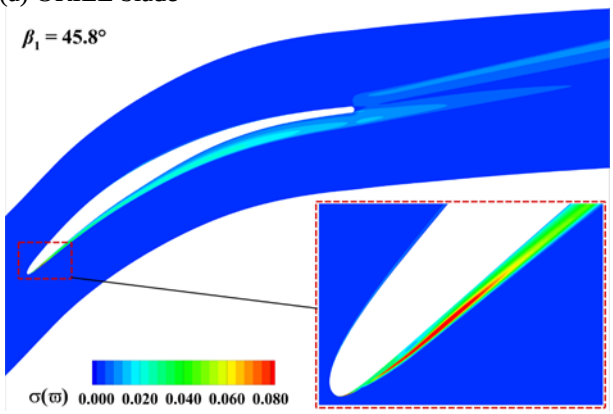

(b) ASYLE blade

Fig. 13 Distributions of $\sigma(\varpi)$ for the ORILE blade and ASYLE blade β_1=45.8°

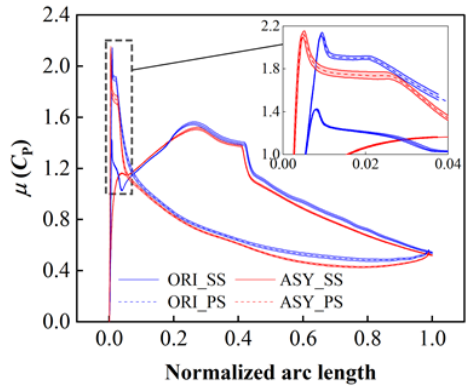

(a) Distributions of $\mu(C_P)$

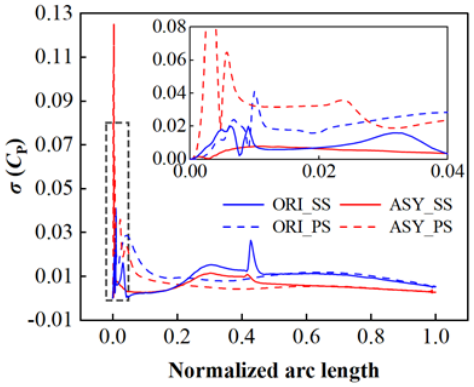

(b) Distributions of $\sigma(C_P)$

Fig. 14 Static pressure coefficient C_P characteristics comparison at β_1=45.8°

As shown in Fig.13, the high variation zone of ϖ is mainly concentrated in the pressure surface side flow and wake mixing region. The value of $\sigma(\varpi)$ decreases from LE to the downstream, which indicates that the LE region flow is most evidently affected by uncertain profile errors. At β_1=45.8°, the high $\sigma(\varpi)$ region range of ASYLE is much smaller than that of ORILE; thus, the variation caused by LE flow is less, and the impacts spread downstream are slighter.

Figure 14 shows the distribution characteristics of the static pressure coefficient C_P along the blade surface with the profile error uncertainties at β_1=45.8°. Since 45.8° is below the design inflow angle β_{1des}, the operating condition is at negative incidence, and the stagnation point is above the LE point. Consequently, the spikes of the static pressure coefficient mean value $\mu(C_P)$ are much more apparent at the pressure side leading edges (PSLE) for both blades in Fig.14(a) and play a key role in the LE flows. While the extremum values of PSLE spike intensities for both blades are similar, the subsequent platform distribution of ASYLE is significantly lower than that of ORILE, which indicates that the size of the PSLE separation bubble is smaller, and LE separation flow causes less effect downstream. This result also explains why the propagation effect of ORILE flow is more noticeable in Fig.13. Moreover, the suction side leading edge (SSLE) suction spike of ASYLE remains lower than that of ORILE, which indicates that ASYLE remains superior in controlling excessive acceleration and weakening the suction spike intensity for SSLE flow.

Moreover, $\sigma(C_P)$ in Fig.14(b) for each blade has a two-peak distribution at the initial position, corresponding to the acceleration zone of LE flow and the large curvature profile area. The value as well as variation of $\sigma(C_P)$ for ASYLE is higher because its PSLE profile curvature is larger and more easily changed with the profile geometry. As Fig.13 shows, $\sigma(\varpi)$ in the acceleration area is indistinct for both blades, such that we infer that the variation in the suction spike is not the direct cause of performance dispersion under uncertain profile errors. The $\sigma(C_P)$ of the ASLYE pressure side remains higher than that of the ORILE blade until x/a=0.027, which is the maximum thickness position of the separation bubble as well as the start of the LE transition. Afterwards, the pressure surface side C_P variations of the ASYLE blade remain much lower.

For the suction surface side, the C_P of the two blades differ little in the LE region, but the C_P distribution for ASYLE is more uniform. This occurs because there is still obvious acceleration of the ORILE blade SSLE flow, leading to a higher suction spike intensity. Therefore, there is also a two-peak $\sigma(C_P)$ distribution of the ORILE blade SSLE flow. From x/a=0.2, the surface C_P variation of the ORILE blade is significantly higher than that of the ASYLE blade. In addition, both of the blades clearly have a spike at approximately x/a=0.4, which corresponds to the positions of the platform areas of $\mu(C_P)$ in Fig.14(a). These are the positions of the separation transition on the suction surfaces of the blade. This indicates that the profile error

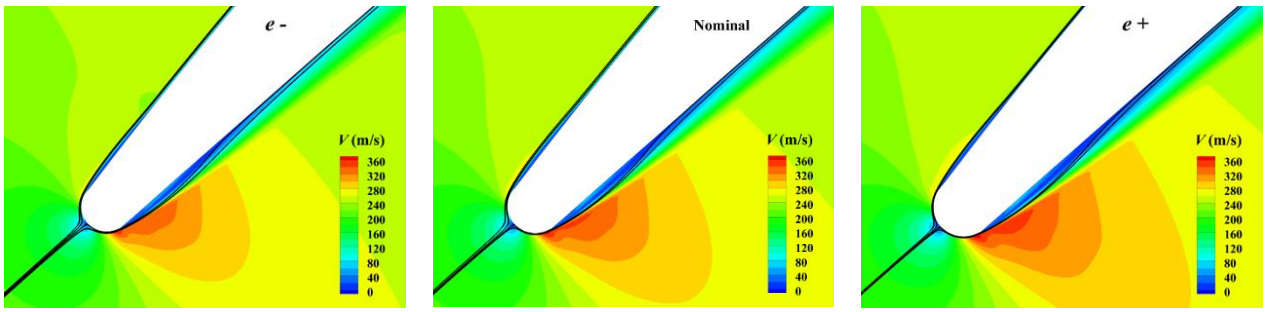

(a) ORILE blade

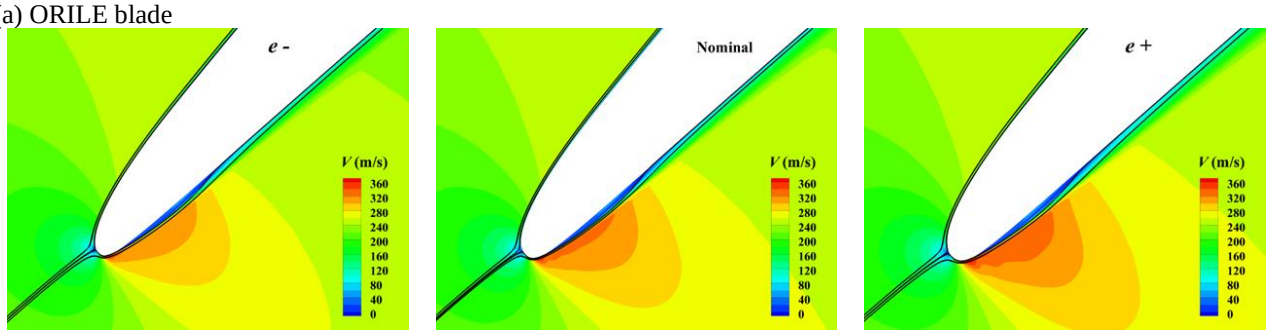

(b) ASYLE blade

Fig. 15 Velocity distribution maps around the leading edge at β_1=45.8°

has a great influence on the separation transition region, and the ASYLE can reduce this effect.

The above discussion indicates that the variation in suction spike is not the main cause for performance dispersion under uncertain profile errors. To define the major influence mechanism, the velocity distribution maps and streamlines around LE at β_1=45.8° are presented in Fig.15. Three profiles with different errors for each blade are displayed, and the profile with negative error is marked as "*e*-", while the profile with positive error is marked as "*e*+".

It is evident that the velocity variation at the PSLE acceleration zone of ASYLE is greater, although the velocity values are smaller than those of ORILE. This occurs because there is a particular region of a large curvature curve on the pressure surface side of the ASYLE, which is a typical characteristic of the ASYLE, because the moderation of SSLE curvature comes from the compression of the PSLE space. Consequently, the acceleration region of the pressure surface side for ASYLE is more clearly affected by the profile errors. This effect accounts for the phenomenon in Section 5.2 that the σ(CP) of ASYLE is slightly higher in the acceleration region.

Furthermore, separation bubbles appear on PSLE for both blades at β1=45.8°, and the separation bubble size of the ORILE blade is much larger than that of the ASYLE blade. In addition, the variation in the separation bubble geometric size of ORILE is more evident. To make a clearer comparison of the geometric size of the separation bubbles, Fig.16 shows the quantitative evaluation of the length and maximum thickness of separation bubbles of two blades withdifferent profile errors at β_1=45.8°. The size of the ASYLE separation bubble remains smaller than that of ORILE, and it introduces less disturbance to LE and downstream flow. Clearly, the ORILE separation bubble size varies more with the change in profile errors;

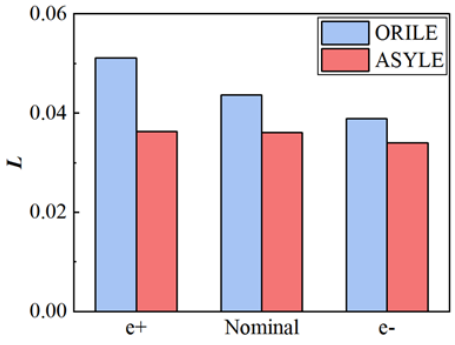

(a) Separation bubble length *L*

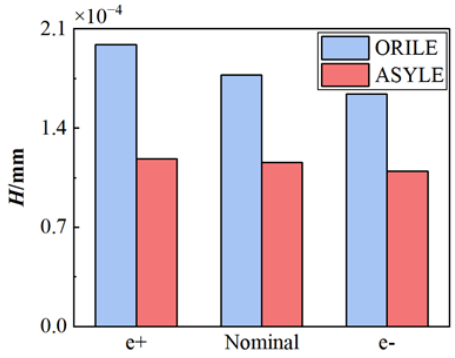

(b) Separation bubble maximum thickness *H*

Fig. 16 Comparison of separation bubble geometric size

therefore, the influence on the LE flow field is more uncertain.

In addition, analysis of Fig.13 shows that the high $\sigma(\varpi)$ areas are associated with the positions of separation bubbles. Furthermore, we observe that the initial positions of the high $\sigma(\varpi)$ areas are the locations of the maximum thickness of the separation bubbles and develop along the

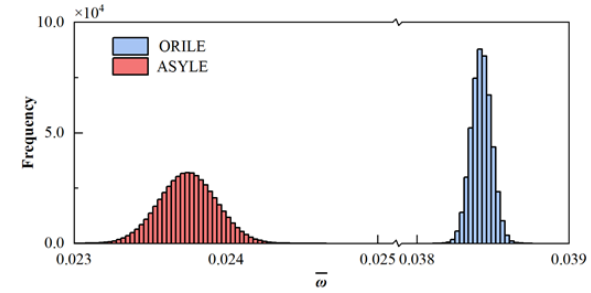

(a) β_1 = 47.8°

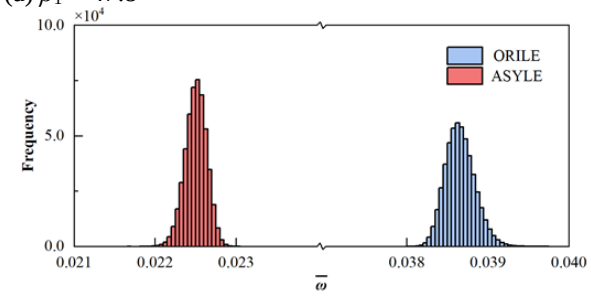

(b) β_1 = 48.8°

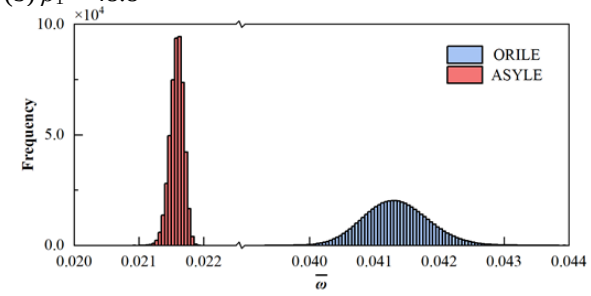

(c) β_1 = 49.8°

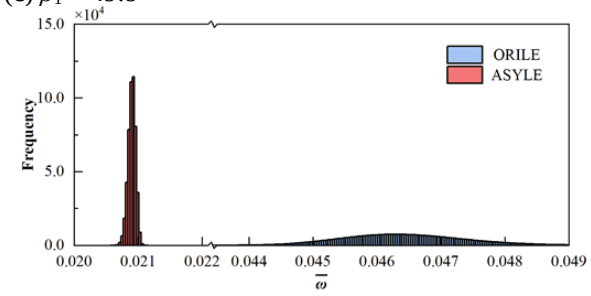

(d) β_1 = 50.8°

Fig. 17 Frequency distribution comparison of performance under inlet flow perturbations

outer edge of the separation bubbles. Moreover, the PSLE $\sigma(C_P)$ of ORILE starts to surpass that of ASYLE at x/a=0.027, which is also the maximum thickness position of the separation bubble. Consequently, inferences can be drawn that the uncertainty of the LE flow under profile error is mainly caused by the variation in the geometry of the LE separation bubble, especially the maximum thickness of the separation bubble.

Overall, the ASLYE increases the curvature of the pressure surface side, so the accelerated velocity variation caused here fluctuates greatly at small inflow angles. However, this effect is not the key factor in the LE flow uncertainties. Compared with the LE accelerated velocity fluctuation, the influence caused by the separation bubble structure variation is much more severe for profile errors and then spreads downstream.

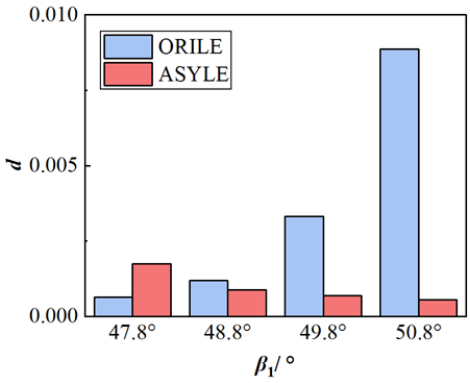

Fig. 18 Performance dispersibility comparison under uncertain inflow angle perturbations

6. INFLUENCE OF UNCERTAIN INFLOW ANGLE PERTURBATIONS ON AERODYNAMIC ROBUSTNESS

6.1 Influence of Uncertain Inflow Angle Perturbations on Performance Characteristics

The intended low loss operating ranges from β_1=47.8° to 50.8° of the ASYLE blade were taken into study. To investigate the specific performance output of the ASYLE blade under inflow angle perturbations, the frequency distribution histogram graphs of ϖ are also given in Fig.17 and are compared with the ORILE blade. The results were derived through the NIPC model built at inlet flow conditions as described in Section 4.2. The figure clearly shows that at β_1=47.8°, the performance distribution of the ASYLE blade is more dispersed, which means that in this case, the ASYLE blade is more affected by the inflow angle perturbations. However, when the inflow angle β_1 becomes larger from β_1=48.8° to 50.8°, the performance of the ASYLE blade becomes increasingly concentrated. We thus conclude that the ASYLE blade is evidently more robust at large inflow angles.

The quantitative performance dispersibility $d(\varpi)$ comparison is presented in Fig.18. The performance dispersibility difference caused by uncertain inflow angle perturbations is relatively inapparent at small inflow angles but is greatly evident at a larger inflow angle β_1 = 50.8°, and the total pressure loss dispersion of the ASYLE blade decreases by 93.8% relative to that of the ORILE blade. Consequently, the robustness of ASYLE is better overall compared with ORILE.

A comparison of the total pressure loss statistical mean value $\mu(\varpi)$ of the ORILE blade and ASYLE blade under uncertain inflow angle perturbations is given in Fig.19(a), and the standard deviation of the total pressure loss $\sigma(\varpi)$ comparison is given in Fig.19(b). As shown in the figure, the $\mu(\varpi)$ of the ASYLE blade remains much smaller than that of the ORILE blade under inflow angle uncertainty. However, the $\sigma(\varpi)$ of the ASYLE blade is not always lower than that of the ORILE blade. As the inflow angle β_1 increases, the $\sigma(\varpi)$ of the ORILE blade becomes larger, while the $\sigma(\varpi)$ of the ASYLE blade decreases, and the difference becomes evident. This means that in the range of β_1=47.8° to 50.8°, the ASYLE blade shows better

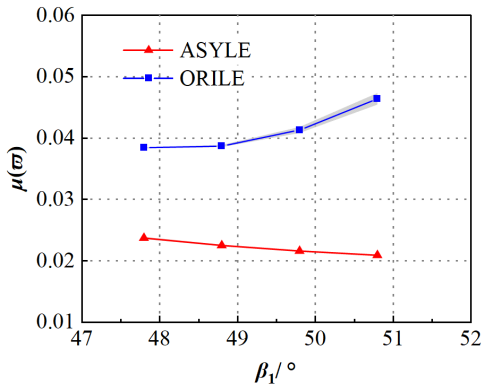

(a) Mean value of total pressure loss $\mu(\varpi)$ comparison

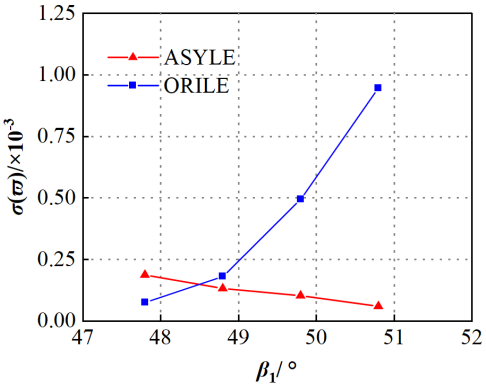

(b) Standard deviation of total pressure loss $\sigma(\varpi)$ comparison

Fig. 19 Comparison of total pressure loss characteristics under uncertain inflow angle perturbations

overall robustness under uncertain inflow angle perturbations, especially at larger inflow angles, which is opposite to how robustness is influenced by profile error. The ASYLE blade significantly diminishes the influence of uncertain inflow angles at higher β_1, and the $\sigma(\varpi)$ of the ASYLE blade is reduced by 93.7% at β_1 = 50.8° compared with the ORILE blade.

We infer that the ASYLE is not as sensitive as conventional wisdom supposes under uncertain inflow angle perturbations and is more robust at larger inflow angles. In addition, Fig.19 also reveals that the deviations of the total pressure loss are associated with the mean value. For each blade, the larger the mean value $\mu(\varpi)$ is, the larger the deviation $\sigma(\varpi)$ would be.

6.2 Influence of Uncertain Inflow Angle Perturbations on the Flow Field and Mechanism Analysis

According to a previous study, the robustness difference of the two blades is less at smaller inflow angles but is especially evident at larger inflow angles. The influential effects of inflow angle uncertainties are closely related to the working conditions. To examine the difference in the propagation from inflow angle uncertainties in the flow field, the distribution of the total pressure loss standard deviation $\sigma(\varpi)$ at β_1=50.8° is presented in Fig.20.

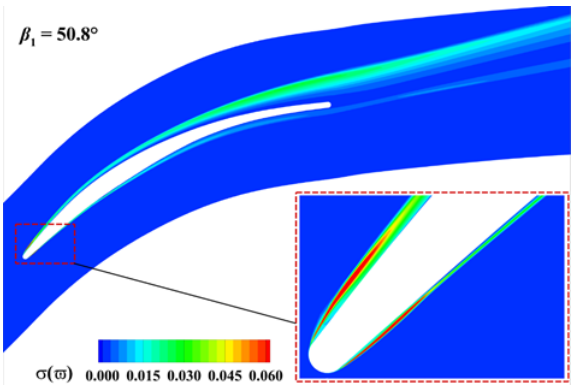

(a) ORILE blade

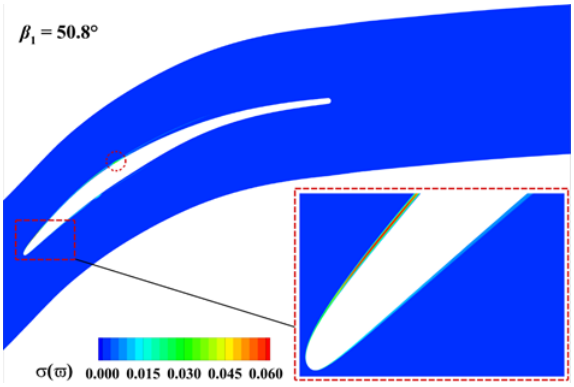

(b) ASYLE blade

Fig. 20 Distributions of $\sigma(\varpi)$ for the ORILE blade and ASYLE blade at β_1=50.8°

As shown, the variation zone of ϖ is mainly concentrated in the suction surface side flow and wake. Similarly, the highest value of $\sigma(\varpi)$ comes from the LE region. This also shows that the LE flow is most directly affected by the uncertain inflow angle perturbations. Apparently, the LE flow field deviation of the ASYLE blade is much less than that of the ORILE blade at β_1=50.8°; thus, the variation caused by its LE flow is less, and the spread of impacts to the downstream area is negligible.

Figure 21 shows the distribution characteristics of the static pressure coefficient C_P along the blade surface with inflow angle uncertainties at β_1=50.8°. Because 50.8° is above the design inflow angle β_{1des}, the operating condition is at positive incidence. Consequently, the spikes of the static pressure coefficient mean value $\mu(C_P)$ are much more apparent at SSLE for both blades in Fig.21(a) and play a key role in the LE flows. Under uncertain inflow angle perturbations, the statistical suction spike intensity of ASYLE remains smaller than that of ORILE, so the acceleration and overexpansion of LE flow can be better controlled, which helps to avoid LE transition and reduction of boundary layer momentum. In addition, the comparison of SSLE $\mu(C_P)$ shows that the platform distribution comes out at x/a=0.01 of ORILE, which represents the appearance of the LE separation bubble. In contrast, such a distribution is inconspicuous in ASYLE. This indicates that the separation bubble of ASYLE is still restricted under uncertain inflow angle

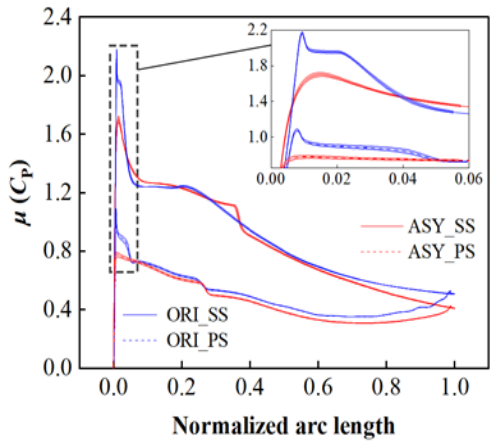

(a) Distributions of $\mu(C_P)$

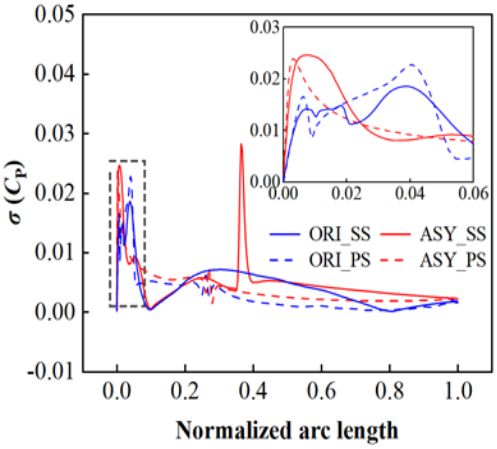

(b) Distributions of $\sigma(C_P)$

Fig. 21 Static pressure coefficient C_P characteristics comparison at β_1=50.8°

perturbations. The difference in separation bubbles for the two blades is also reflected in Fig.20, in which the $\sigma(\varpi)$ of the ORILE separation region is much higher, while the $\sigma(\varpi)$ of ASYLE is indistinctive at SSLE.

Figure 21(b) shows that the distribution trends of SSLE and PSLE $\sigma(C_P)$ are similar for both blades, which means that both the SSLE and PSLE flows are affected by the inflow angle perturbations. Similar to the regularity of the influence of uncertain profile errors, the $\sigma(C_P)$ of ASYLE is higher for the LE acceleration region because the curvature distribution of the ASYLE profile is uneven and the stagnation point varies with the inflow angle perturbations, so the acceleration process is more different than that of ORILE, of which the LE profile curvature is constant. However, as discussed in Sections 5.2 and 5.3, the variation in the LE acceleration region flow is not a key factor for the flow field and performance dispersion under uncertain inflow angle perturbations. Moreover, the $\mu(C_P)$ of the ASYLE blade suction surface has a platform distribution at approximate x/a=0.36, which is the transition position on the suction surface. The $\mu(C_P)$ of the ORILE blade suction surface does not have such a platform, which indicates that there is no transition on the main body surface and that the flow is already fully turbulent after LE flow. The ASYLE blade still has superiority in maintaining laminar boundary flow under uncertain inflow angle perturbations.

The $\sigma(C_P)$ of the ASLYE suction surface side remains higher than that of the ORILE blade until x/a=0.025, which is the maximum thickness position of the separation bubble as well as the start of the LE transition. Then, $\sigma(C_P)$ becomes closer at x/a=0.055, which is the attachment position of the separation bubble. This implies that variation in the separation bubble size is inevitable for ORILE blades with inflow angle uncertainties.

It is noticeable that there is a $\sigma(C_P)$ peak of the ASYLE blade suction surface at x/a=0.36. That is, the position of the separation transition on the blade body surface. It can also be observed in Fig.20(b) that a high value of $\sigma(\varpi)$ appears at the corresponding spot of the ASYLE blade body suction surface. This is because the separation transition position at this location shifts with the variation of inflow angles, leading to the deviation of C_P. Such a phenomenon does not exist for the ORILE blade because the flow has already transitioned into turbulent in the LE region, and there is no more transition process on the blade body surface.

To explore the major influence mechanism of uncertain inflow angle perturbations, the velocity distribution maps and streamlines around LE at β_1=50.8° are presented in Fig.22, where the flow fields of three different inflow angle deviations for each blade are displayed. In the data, the negative deviation is marked as "f -"and the positive deviation is marked as "f +".

Figure 22 clearly shows that there are separations at both SSLE and PSLE of ORILE, while there is no separation for ASYLE. The positions of LE separations are associated with the high $\sigma(\varpi)$ areas in Fig.19. We thus infer that the separation bubble is the key factor that results in flow field uncertainties under uncertain inflow angle perturbations. Figure 22(a) shows that the geometric sizes of separation bubbles at SSLE and PSLE of ORILE vary with the inflow angles at the same time, but the SSLE separation bubble is much thicker. Therefore, the variation in the SSLE separation bubble has more impacts on the LE and downstream flow uncertainties.

From the above conclusions, it follows that the variation in separation bubble geometric size is also the direct factor that causes flow field uncertainties as well as performance dispersion under uncertain inflow angle perturbations. Compared to the ORILE blade, since the ASYLE blade eliminates the separation bubble at a higher inflow angle, the flow field uncertainties and performance dispersion are much smaller. Therefore, the ASYLE blade shows better robustness.

7. CONCLUSION

In this paper, the aerodynamic robustness of a compressor blade with a novel ASYLE design under geometric and operational uncertainties is investigated. Two research models for profile error and inflow angle perturbation are established, and the UQ method based on NIPC combined with CFD simulation was implemented to

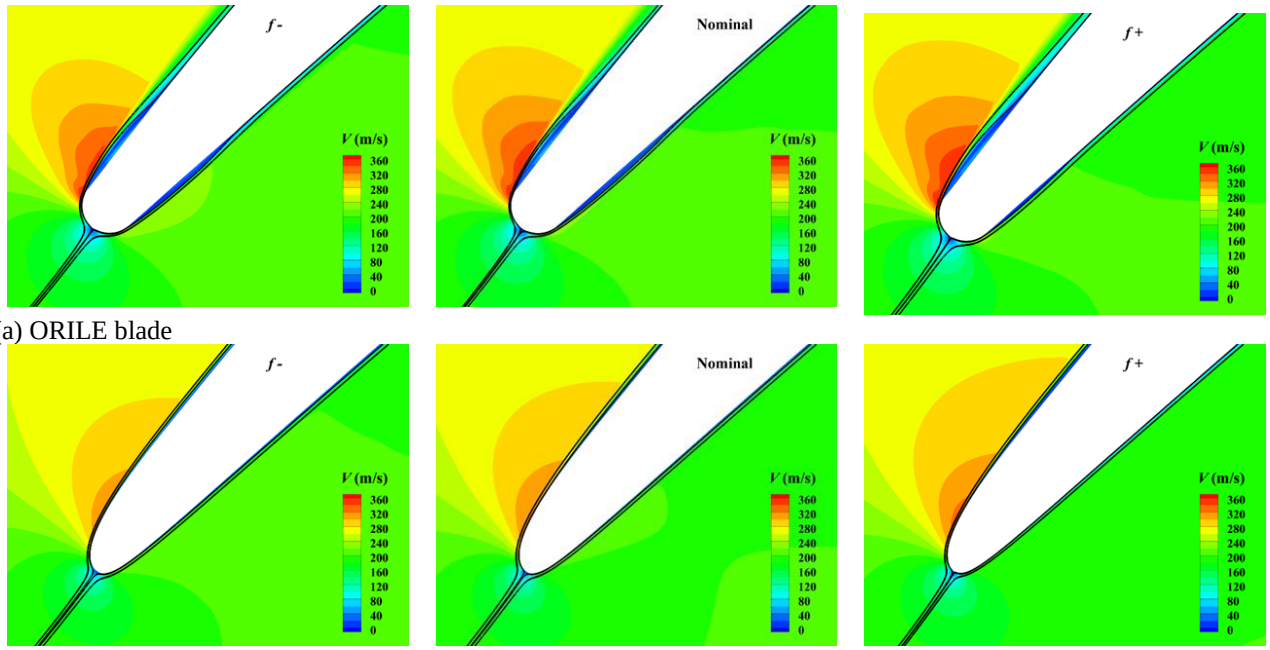

(a) ORILE blade

(b) ASYLE blade

Fig. 22 Velocity distribution maps around the leading edge at β_1=50.8°

study the robustness of the ASYLE blade with comparison of the ORILE blade under these two kinds of uncertainties. The resulting analysis reveals that the aerodynamic robustness of the ORILE blade is improved rather than reduced by the ASYLE design. Our main conclusions are as follows:

1) Considering the uncertain profile errors, the ASYLE blade shows better aerodynamic robustness than the ORILE blade. The total pressure loss mean value of the ASYLE blade remains lower, and the operating range is extended by 2.3°. The ASYLE blade is more robust to profile errors, especially at smaller inflow angles. At β_1=45.8°, the dispersion of the total pressure loss $d(\varpi)$ of the ASYLE blade is reduced by 53.1%, and $\sigma(\varpi)$ is reduced by 53.8% compared with the ORILE blade. The variations caused by profile error uncertainty mainly affected the pressure surface side flow field, which starts at the maximum thickness of the PSLE separation bubble and spreads downstream. Compared with ORILE, the geometric size change of the ASYLE blade is less, so the flow uncertainties are relatively minor.

2) Regarding the uncertain inflow angle perturbations, the ASYLE blade has better statistical performance and robustness, especially at larger inflow angle conditions. At β_1=50.8°, the dispersion of the total pressure loss $d(\varpi)$ of the ASYLE blade can be reduced by up to 93.8%, and $\sigma(\varpi)$ is reduced by 93.7% compared with ORILE. The ASYLE is still able to prevent the LE transition under inflow angle uncertainty. The variations caused by uncertain inflow angles initiate at the LE separation bubbles and propagate downstream. Compared with the ORILE, the ASYLE eliminates the separation bubble at a higher inflow angle, and the flow field uncertainties and performance dispersion are much smaller. Thus, the ASYLE blade shows better robustness than the ORILE blade.

3) Considering both kinds of uncertainties, the variations in the LE separation bubble are the direct causes of the flow field uncertainties and performance dispersion. Although the acceleration process of ASYLE flow is more clearly affected than that of ORILE flow because the ASYLE blade has better control over the LE separation bubble size. Thus, the ASYLE design reduces the sensitivity of LE separation flow and can improve the aerodynamic robustness. We infer that to carry out robust LE design, it is necessary to pay attention to the LE separation flow control and reduce the sensitivity of LE separation bubble variations to uncertainties.

ACKNOWLEDGEMENTS

The authors gratefully acknowledge the support of the National Natural Science Foundation of China (No.51790512, No.92152301), the National Science and Technology Major Project of China (No. J2019-II-0016-0037), the Innovation Foundation for Doctoral Dissertation of Northwestern Polytechnical University (No.CX2021073), and the Ministry of Education of the People's Republic of China (111Project; No. B17037).

CONFLICT OF INTEREST

The authors declare that they have no known competing financial interests or personal relationships that could have appeared to influence the work reported in this paper.

AUTHORS CONTRIBUTION

G. Yang and **L. Gao** designed research; **G. Yang**, **C. Ma** and **H. Wang** developed the method; **G. Yang** and **N. Ge** collected the data; **G. Yang** analysed the data; **G. Yang** and **L. Gao** wrote the paper.

REFERENCES

Ali, Q. S., & Kim, M. H. (2020). Unsteady aerodynamic performance analysis of an airborne wind turbine under load varying conditions at high altitude. *Energy Conversion and Management*, *210*, 112696. https://doi.org/10.1016/j.enconman.2020.112696.

Carter, A. D. S. (1961). Blade profiles for axial flow fans, pumps and compressors, etc. unpacking the unique relationship between set for variability and word reading development: examining word- and child-level predictors of performance. *Proceedings of the Institution of Mechanical Engineers*, *175*(1), 775–806. https://doi.org/10.1243/PIME_PROC_1961_175_051

Cui, T., Wang, S., Tang, X., Wen, F., & Wang, Z. (2019). Effect of leading-edge optimization on the loss characteristics in a low-pressure turbine linear cascade. *Journal of Thermal Science*, *28*, 886–904. https://doi.org/10.1007/s11630-019-1196-3

Cumpsty, N. A. (2004). *Compressor aerodynamics*. Longman Scientific & Technical.

Gao, L., Ma, C., & Cai, Yu. (2019). A robust blade design method based on non-intrusive polynomial chaos considering profile error. *Journal of Thermal Science*, *28*(9), 875-885. https://doi.org/10.1007/s11630-019-1185-6

Gao, L., Ma, C., Cai, M., Li, R., Wang, H., & Yang, G. (2022). Influence of uncertain inflow conditions on a subsonic compressor cascade based on wind tunnel experiment. *Proceedings of the Institution of Mechanical Engineers, Part C: Journal of Mechanical Engineering Science*, *236*(15), 8285-8299. https://doi.org/10.1177/09544062221087584

Gao, L., Wang, H., Yang, G., Ma, C., Huang, P., & Tang, K. (2023). Discussion on machining defects of blade leading edge and aerodynamic qualification. *Journal of Propulsion Technology*, *44*(1), 81-90. https://doi.org/10.13675/j.cnki.tjjs.22010031

Garzón, V. E. (2002). *Probabilistic aerothermal design of compressor airfoils.* [Doctoral dissertation, Massachusetts Institute of Technology].

Goodhand, M. N. (2010). *Compressor leading edges.* [Doctoral dissertation, Cambridge University].

Goodhand, M. N., & Miller, R. J. (2009). Compressor leading edge spikes: a new performance criterion. *Journal of Turbomachinery*, *133*(2), 021006. https://doi.org/10.1115/1.4000567

Goodhand, M. N., Miller, R. J., & Lung, H. W. (2012, June 11-15) *The sensitivity of 2d compressor incidence range to in-service geometric variation*. [Conference session]. Proceedings of the ASME Turbo Expo 2012: Turbine Technical Conference and Exposition. Volume 8: Turbomachinery, Parts A, B, and C. Copenhagen, Denmark. 159-170. https://doi.org/10.1115/GT2012-68633

Goodhand, M. N., Miller, R. J., & Lung, H. W. (2015). The impact of geometric variation on compressor two-dimensional incidence range. *Journal of Turbomachinery*, *137*(2), 021007. https://doi.org/10.1115/1.4028355

Guo, Z., Chu, W., & Zhang, H. (2022). A data-driven non-intrusive polynomial chaos for performance impact of high subsonic compressor cascades with stagger angle and profile errors. *Aerospace Science and Technology*, *129*, 107802. https://doi.org/10.1016/j.ast.2022.107802

Guo, Z., Chu, W., & Zhang, H. (2023). Effects of inlet incidence perturbations on compressor cascade performance using adaptive sparse grid collocation. *Journal of Applied Fluid Mechanics*, *16*(6), 1281-1295. https://doi.org/10.47176/jafm.16.06.1638

Hamakhan, I. A., & Korakianitis, T. (2010). Aerodynamic performance effects of leading-edge geometry in gas-turbine blades. *Applied Energy*, *87*(5), 1591-1601. https://doi.org/10.1016/j.apenergy.2009.09.017

Hanson, R. E., Buckley, H. P., & Lavoie, P. (2012). Aerodynamic optimization of the flat-plate leading edge for experimental studies of laminar and transitional boundary layers. *Experiments in Fluids*, *53*(4), 863-871. https://doi.org/10.1007/s00348-012-1324-2

Langtry, R. B., Menter, F. R., Likki, S. R., Suzen, Y. B., Huang, P. G., & Völker, S. (2004). A correlation-based transition model using local variables—part ii: test cases and industrial applications. ASME. *Journal of Turbomachinery*, 423-434. https://doi.org/10.1115/1.2184353

Lejon, M., Andersson, N., Ellbrant, L., & Mårtensson, H. (2020). The impact of manufacturing variations on performance of a transonic axial compressor rotor. *Journal of Turbomachinery*, *142*(8), 081009. https://doi.org/10.1115/1.4046617

Li, R., Gao, L., Zhang, S., Li, Y., & Gao, T. (2018). Application of shear-sensitive liquid crystal coating to visualization of transition and reattachment in compressor cascade. *Chinese Journal of Aeronautics*, *31*(11), 2073-2079. https://doi.org/10.1016/j.cja.2018.06.003

Liu, B., Yuan, X., & Yu, X. (2013). Effects of leading-edge geometry on aerodynamic performance in controlled diffusion airfoil. *Journal of Propulsion Technology*, *34*(7), 890-897. https://doi.org/10.13675/j.cnki.tjjs.2013.07.006

Liu, H., Liu, B., Li, L., & Jiang, H. (2003, June 16–19). *Effect of leading-edge geometry on separation bubble on a compressor blade* [Conference session]. Proceedings of the ASME Turbo Expo 2003, collocated with the 2003 International Joint Power Generation Conference. Parts A and B, Atlanta, Georgia, USA. 387-395. https://doi.org/10.1115/GT2003-38217

Liu, J., Yu, X., Meng, D., Shi, W., & Liu, B. (2021). State

and effect of manufacture deviations of compressor blade in high-pressure compressor outlet stage. *Acta Aeronautica et Astronautica Sinica*, *42*(2), 423796. https://doi.org/10.7527/S1000-6893.2020.23796

Lu, H., & Xu, L. (2003). Circular leading edge with a flat for compressor blades. J*ournal of Propulsion Technology*, *24*(6), 532-536. https://doi.org/10.13675/j.cnki.tjjs.2003.06.014

Ma, C., Gao L., & Cai, Y. (2017, June 26–30). *Robust optimization design of compressor blade considering machining error*. Proceedings of the ASME Turbo Expo 2017: Turbomachinery Technical Conference and Exposition. Volume 2C: Turbomachinery. Charlotte, North Carolina, USA. V02CT47A003. ASME. https://doi.org/10.1115/GT2017-63157

Ma, C., Gao, L., Wang, H., Li, R., & Wu, B. (2021). Influence of leading edge with real manufacturing error on aerodynamic performance of high subsonic compressor cascades. *Chinese Journal of Aeronautics*, *34*(6), 220-232. https://doi.org/10.1016/j.cja.2020.08.018

Menter, F. R., Langtry, R. B., Likki, S. R., Suzen, Y. B., Huang, P. G., & Völker, S. (2004). A correlation-based transition model using local variables—part i: model formulation. *Journal of Turbomachinery*. 413-422. https://doi.org/10.1115/1.2184352

Nicholls, S., Shaw, W., & Hauf, T. (1983). An intercomparison of aircraft turbulence measurements made during JASIN. *Journal of Applied Meteorology and Climatology*, *22*(9), 1637-1648. https://doi.org/10.1175/1520-0450(1983)022<1637:AIOATM>2.0.CO;2

Song, Y., Gu, C., & Xiao, Y. (2014). Numerical and theoretical investigations concerning the continuous-surface-curvature effect in compressor blades. *Energies*, *7*(12), 8150-8177. https://doi.org/10.3390/en7128150

Walraevens, R. E., & Cumpsty, N. A. (1995). Leading edge separation bubbles on turbomachine blades. *Journal of Turbomachinery*, *117*(1), 115-125. https://doi.org/10.1115/1.2835626

Wang, H., Gao, L., Yang, G., & Wu, B. (2023). A robust data-driven uncertainty quantification method and its application in compressor cascade. *Acta Aeronautica et Astronautica Sinica*, *44*, 628169. https://doi.org/10.7527/S10006893.2023.28169

Wheeler, A. P. S., & Miller, R. J. (2008, June 9-13). *Compressor wake/leading-edge interactions at Off design incidences.* [Conference session]. Proceedings of the ASME Turbo Expo 2008: Power for Land, Sea, and Air. Volume 6: Turbomachinery, Parts A, B, and C, Berlin, Germany. 1795-1806. https://doi.org/10.1115/GT2008-50177

Wheeler, A. P. S., Sofia, A., & Miller, R. J. (2009). The effect of leading-edge geometry on wake interactions in compressors. *Journal of Turbomachinery*, *131*(4), 041013. https://doi.org/10.1115/1.3104617

Yang, G., Gao, L., Wang, H., & Cai, M. (2021) Asymmetric leading edge design of diffusion cascade based on NURBS. *Journal of Aerospace Power*, *36*(03), 655-663. https://doi.org/10.13224/j.cnki.jasp.2021.03.021

Yang, G., Gao, L., Wang, H., & Chang, L. (2022). Influence of leading edge point on aerodynamic performance of asymmetric leading edge compressor airfoils. *International Journal of Turbo & Jet-Engines*. https://doi.org/10.1515/tjj-2021-0054.

Yang, G., Gao, L., Zhao, L., & Lin, S. (2020). Effect of asymmetric leading edge on aerodynamic performance of diffusion cascade. *Journal of Engineering Thermophysics*, *41*(10), 75-80.

Zhang, W., Zou, Z., & Ye, J. (2012). Leading-edge redesign of a turbomachinery blade and its effect on aerodynamic performance. *Applied Energy*, *93*, 655-667. https://doi.org/10.1016/j.apenergy.2011.12.091